P- and T-Wave Delineation in ECG Signals Using a Bayesian Approach and a Partially Collapsed Gibbs Sampler

Chao Lin*, *Student Member, IEEE*, Corinne Mailhes, *Member, IEEE*, and Jean-Yves Tourneret, *Senior Member, IEEE*

***Abstract*—Detection and delineation of P- and T-waves are important issues in the analysis and interpretation of electrocardiogram (ECG) signals. This paper addresses this problem by using Bayesian inference to represent *a priori* relationships among ECG wave components. Based on the recently introduced partially collapsed Gibbs sampler principle, the wave delineation and estimation are conducted simultaneously by using a Bayesian algorithm combined with a Markov chain Monte Carlo method. This method exploits the strong local dependency of ECG signals. The proposed strategy is evaluated on the annotated QT database and compared to other classical algorithms. An important feature of this paper is that it allows not only for the detection of P- and T-wave peaks and boundaries, but also for the accurate estimation of waveforms for each analysis window. This can be useful for some ECG analysis that require wave morphology information.**

***Index Terms*—Bayesian analysis, electrocardiogram, Markov chain Monte Carlo method.**

I. Introduction

THE ANALYSIS of electrocardiograms (ECGs) has received increasing attention because of its vital role in many cardiac disease diagnoses. Most of the clinically useful information in ECGs can be obtained from the intervals, amplitudes, or wave morphology of the ECGs. Therefore, the development of efficient and robust methods for automatic ECG delineation is a subject of major importance. The QRS complex is the most characteristic waveform of the ECG signal. Its high amplitude makes QRS detection easier than other waves. Thus, it is generally used as a reference within the cardiac cycle. Algorithms for P- and T-wave detection and delineation (determination of peaks and limits of the individual P and T waves) usually begin with QRS detection. Search windows are then defined before and after the QRS location to seek for the other waves. Finally, an appropriate strategy is used to enhance the distinctive features of each wave in order to find its peaks and limits.

Manuscript received March 11, 2010; revised May 23, 2010, August 26, 2010, and September 6, 2010; accepted September 6, 2010. Date of publication September 16, 2010; date of current version November 17, 2010. *Asterisk indicates corresponding author.*

*C. Lin is with the TéSA Laboratory, University of Toulouse, Toulouse 31071, France (e-mail: chao.lin@tesa.prd.fr).

C. Mailhes and J.-Y. Tourneret are with the Institut de recherche en informatique de Toulouse (IRIT, UMR 5505 of the CNRS), University of Toulouse, Toulouse 31071, France (e-mail: Corinne.Mailhes@enseeiht.fr; Jean-Yves.Tourneret@enseeiht.fr).

Color versions of one or more of the figures in this paper are available online at http://ieeexplore.ieee.org.

Digital Object Identifier 10.1109/TBME.2010.2076809

One can find in the literature many different P- and T-wave delineation approaches [1]–[19]. A first class of algorithms is based on filtering techniques, such as adaptive filtering [1], low-pass differentiation (LPD) [2], and nested median filtering [3]. A second class of methods applies a basis expansion technique to the ECG signal and uses the resulting coefficients for detecting P- and T-waves. The different basis functions that have been considered in the literature include discrete Fourier transform [4], discrete cosine transform [5], and wavelet transform (WT) [6], [7]. A third class of approaches considers classification and pattern recognition methods, such as fuzzy theory [8], artificial neural networks [9], pattern grammars [10], and hidden Markov models [11]. Delineation can also be based on the concept of fitting a realistic model to the ECG and extracting parameters from the model to determine waveform onsets and offsets. Particular attention has been devoted to Gaussian mixture models whose parameters can be estimated with nonlinear gradient descent [12] or Kalman filters (KFs) [13], [14]. Finally, we would like to mention other delineation strategies based on length transformation [15], uniform thresholding [16], approximating function theory [17], and characterization of TU complexes [18]. Note that some of these methods can only be used to obtain a subset of P- and T-wave characteristic points. Due to the low slope and low magnitude of P- and T-waves and due to the lack of a universal rule to locate the beginning and the end of wave components, P- and T-wave delineation remains a complicated task. Furthermore, in addition to the estimation of wave peaks and limits, an accurate waveform estimation is certainly relevant for some medical diagnoses (such as T-wave alternans (TWA) detection [20]) or pathology analysis (such as arrhythmia detection [21]).

In this paper, we introduce a novel hierarchical Bayesian model that simultaneously solves the P- and T-wave delineation task and the pointwise waveform-estimation problems. This model takes into account appropriate prior distributions for the unknown parameters (wave locations and amplitudes, and waveform coefficients). These prior distributions are combined with the likelihood of the observed data to provide the posterior distribution of the unknown parameters. The posterior distribution depends on hyperparameters that can be fixed *a priori* or estimated from the observed data. This paper will consider both possibilities depending on the available information regarding these hyperparameters. To alleviate numerical problems related to the posterior associated to the P- and T-wave delineation, we propose to resort to Markov chain Monte

Carlo (MCMC) methods [22]. MCMC is a powerful sampling strategy, appropriate to solve complex Bayesian inference problems. This paper concentrates on a particular MCMC method referred to as partially collapsed Gibbs sampler (PCGS) whose convergence properties have been studied in [23]. The PCGS has shown interesting properties for electromyography (EMG) [24] and optical coherence tomography (OCT) [25], [26]. However, to the best of our knowledge, this is the first application of PCGS to P- and T-wave delineation of ECG signals. The ECG state sequence is Markovian, since the current state (P-wave, QRS complex, and T-wave) only depends on the previous state. This property motivates our study of a PCGS imposing a strong local dependency on the wave locations. The local dependency improves the convergence and the computational efficiency of the sampler.

This paper is organized as follows. The ECG preprocessing considered in this paper is presented in Section II. Section III describes the different elements of the hierarchical Bayesian model that will be used to solve the P- and T-wave delineation problems. Section IV studies a PCGS that generates samples distributed according to the posterior of the proposed hierarchical Bayesian model. The generated samples will be used to estimate the unknown model parameters and hyperparameters. The wave detection and delineation criteria based on the posterior distributions are also presented. Simulation results performed on the standard annotated QT database (QTDB) [27] as well as a comparison with other algorithms are given in Section V. Finally, conclusion is reported in Section VI.

II. Preprocessing

It is common to view ECGs as the combination of two elements, namely, QRS complexes and non-QRS regions. The interval between each successive pair of QRS offset and the subsequent QRS onset constitutes a non-QRS region. Due to the nonstationary nature of ECGs, detection and estimation must involve a limited set of consecutive beats. In the proposed method, we first detect QRS complexes that are the most prominent components of the ECG signal, and then we shift a nonoverlapping D-beat processing window to cover the whole signal. In the processing window, detected QRS complexes become a reference for detecting P- and T-waves. We define a T-search and a P-search regions for each beat, relative to the QRS complex boundaries depending on a recursively computed RR interval. The T- and P-search regions within the processing window are then extracted individually to form T- and P-wave search blocks. The preprocessing procedure can be summarized as follows.

1) QRS detection: QRS complexes are detected using the algorithm of Pan *et al.* [28] based on digital analysis of the slope, amplitude, and width. The filtering that is done prior to this algorithm is found to be satisfactory. Thus, no additional filtering is required before the delineation of P- and T-waves. Note, however, that any other QRS detection algorithm could be used in this preprocessing step.

2) Removal of baseline drift: In the proposed algorithm, waveform coefficients are estimated simultaneously with the wave locations. Baseline drift causes inaccurate waveform-estimation results. For this reason, we employ the method proposed in [29] to remove baseline drift in each RR interval. Note, however, that any other baseline-removal technique could be used in this preprocessing step.

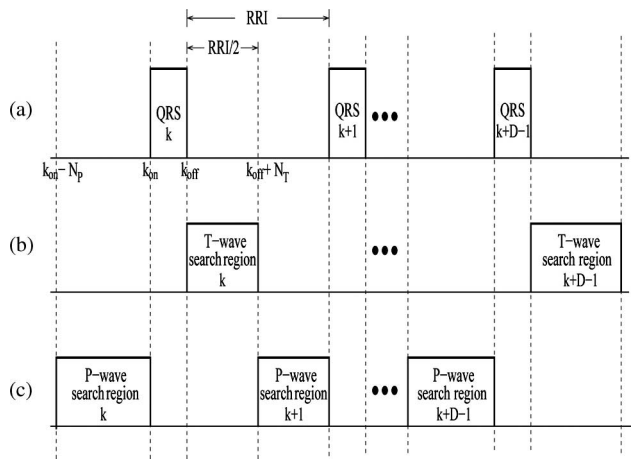

Fig. 1. Preprocessing procedure within the D-beat processing window: (a) Located QRS complexes. (b) T-wave search block. (c) P-wave search block. RRI is the interval from a QRS offset to the next QRS onset, and RRI/2 is half of RRI, here we set $N_T = N_P$ =RRI/2.

3) Construction of P- and T-wave search blocks: As shown in Fig. 1, in the D-beat processing window, D successive right-hand neighborhoods of QRS offsets can be extracted to form a T-wave search block. Suppose that $k_{\rm off}$ denotes a QRS offset location, then a T-wave indicator can only appear in the right-hand neighborhood of $k_{\rm off}$, which can be denoted as $J_T(k_{\rm off}) = (k_{\rm off}+1,\ldots,k_{\rm off}+N_T)$, where N_T denotes the T-wave search region width. Similarly, D left-hand neighborhoods of QRS onsets can be extracted to form a P-wave search block. The length of each search region is fixed according to the current estimated RR interval (denoted by RRI). Thus, it will differ from one beat to another.

The proposed algorithm processes two search blocks (one for T-wave delineation and the other for P-wave delineation) individually using the same Bayesian inference. Section III introduces the Bayesian model applied to T-wave search blocks, while it should be noted that this model is compatible with minor modifications for P-wave search blocks as well.

III. Hierarchical Bayesian Model for T-Waves

Deconvolution models have been widely used in many signal-processing applications including signal segmentation [30], layer detection [25], and EMG signal analysis [31]. Following these ideas, signals in T-wave search blocks are assumed to be the convolution of an unknown impulse response $\mathbf{h} = [h_0,\ldots,h_L]^T$ with an unknown input pulse sequence $\mathbf{u} = [u_1,\ldots,u_M]^T$ such that

$$x_k = \sum_{l=0}^{L} h_l u_{k-l} + n_k \tag{1}$$

with $k \in \{1,\ldots,K\}$, $K = M + L$ is the block length, x_k is the observed ECG signal, and n_k denotes the additive Gaussian

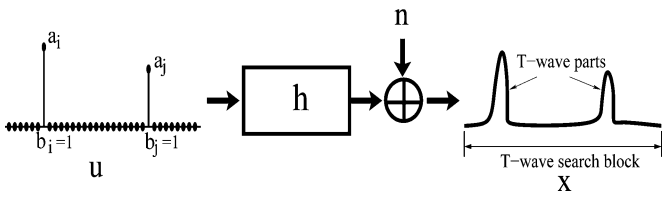

Fig. 2. Modeling of T-wave parts within the T-wave search block.

noise with zero mean and variance σ_n^2. Here, we adopt a zero boundary condition, i.e., the unknown sequence u_m is assumed to vanish for all $m \notin \{1, \ldots, M\}$. In matrix form, (1) can be written as follows:

$$\mathbf{x} = \mathbf{F}\mathbf{u} + \mathbf{n} \tag{2}$$

where $\mathbf{x} = [x_1, \ldots, x_K]^T$, $\mathbf{n} = [n_1, \ldots, n_K]^T$, and $\mathbf{F}$ is the Toeplitz matrix $K \times M$ with first row $[h_0\ \mathbf{0}_{M-1}]$ and first column $\left[\mathbf{h}^T\ \mathbf{0}_{M-1}\right]^T$ ($\mathbf{0}_{M-1}$ is a $(M-1) \times 1$ vector of zeros).

The sequence $\mathbf{u}$ can be further decomposed as a binary sequence $b_m \in \{0, 1\}, m = 1, \ldots, M$ indicating the T-wave existence multiplied by weight factors $\mathbf{a} = [a_1, \ldots, a_M]^T$ representing the T-wave amplitudes, as illustrated in Fig. 2. Note that the impulse response $\mathbf{h}$ is supposed to be unique for D T-wave search regions within the processing window, whereas the amplitudes in $\mathbf{a}$ vary from one region to another. Consequently, (2) can be written as follows:

$$\mathbf{x} = \mathbf{F}\mathbf{B}\mathbf{a} + \mathbf{n} \tag{3}$$

where $\mathbf{B}$ denotes the $M \times M$ diagonal matrix $\mathrm{diag}(\mathbf{b})$ and $\mathbf{b} = [b_1, \ldots, b_M]^T$.

The unknown parameter vector resulting from this reparameterization is $\boldsymbol{\theta} = \left[\mathbf{b}^T, \mathbf{a}^T, \mathbf{h}^T, \sigma_n^2\right]^T$. This paper proposes to estimate the parameter vector $\boldsymbol{\theta}$ by using Bayesian estimation theory. Bayesian inference on $\boldsymbol{\theta}$ is based on the posterior distribution $p(\boldsymbol{\theta}|\mathbf{x}) \propto p(\mathbf{x}|\boldsymbol{\theta})\, p(\boldsymbol{\theta})$ (where $\propto$ means "proportional to"), which is related to the likelihood of the observations and the prior of the parameters. The likelihood $p(\mathbf{x}|\boldsymbol{\theta})$ and the prior $p(\boldsymbol{\theta})$ for the T-wave delineation problem are given below.

A. Likelihood

Using (3), the likelihood of the observed data vector $\mathbf{x}$ can be expressed as follows:

$$p(\mathbf{x}|\boldsymbol{\theta}) = \frac{1}{(2\pi)^{\frac{K}{2}}\, \sigma_n^K} \exp\left[-\frac{1}{2\sigma_n^2} \|\mathbf{x} - \mathbf{F}\mathbf{B}\mathbf{a}\|^2\right] \tag{4}$$

where $\|\mathbf{x}\| = \left(\mathbf{x}^T\mathbf{x}\right)^{\frac{1}{2}}$ denotes the Euclidean norm.

B. Prior Distributions

We propose to model the unknown sequence $u_k = a_k b_k$ as a Bernoulli–Gaussian (BG) sequence

$$b_k \sim \mathcal{B}e(\lambda) \qquad a_k|b_k = 1 \sim \mathcal{N}\left(0, \sigma_a^2\right) \tag{5}$$

where $\mathcal{B}e(\lambda)$ is the Bernoulli distribution with parameter λ such that $p[b_k = 1] = \lambda$. In order to handle both positive and negative wave amplitudes, $a_k|b_k = 1$ is distributed according to a zero mean Gaussian distribution with variance σ_a^2, whereas a_k is not sampled when $b_k = 0$.

Because of the Markov property of ECG, successive T-waves can only appear in search regions located in the right-hand neighborhoods of each QRS offset (whereas P-waves are located to the left-hand neighborhoods of each QRS onset). Thus, the T-wave indicator vector $\mathbf{b}$ cannot have two elements $b_k = 1$ and $b_{k'} = 1$ closer than a minimum-distance constraint d, where d depends on the RR interval length. Consequently, the T-wave detection problem can be seen as a BG blind deconvolution problem with deterministic local constraints, as in [25] and [26]. The prior of $\mathbf{b}$ can then be defined as the product of a minimum-distance constraint indicator function $I_C(\mathbf{b})$ and the likelihood of independent Bernoulli random variables

$$p(\mathbf{b}) \propto \left(\prod_{k=1}^{K} p(b_k)\right) I_C(\mathbf{b})$$

where $I_C(\mathbf{b})$ enforces the minimum-distance constraint $\mathbf{b} \in C$, i.e., $I_C(\mathbf{b}) = 1$ if $\mathbf{b} \in C$ and $I_C(\mathbf{b}) = 0$, if $\mathbf{b} \notin C$.

Since there is no relation between the noise, the impulse response, and the BG sequence σ_n^2, $\mathbf{h}$ and $(\mathbf{b}, \mathbf{a})$ are assigned a priori independent priors such that $p(\boldsymbol{\theta}) = p(\mathbf{b}, \mathbf{a})\, p(\mathbf{h})\, p\left(\sigma_n^2\right)$. The impulse response $\mathbf{h}$, and noise $\mathbf{n}$ are assigned Gaussian priors: $p(\mathbf{h}) = \mathcal{N}\left(\mathbf{0}, \sigma_h^2 \mathbf{I}_{L+1}\right)$; and $p(\mathbf{n}) = \mathcal{N}\left(\mathbf{0}, \sigma_n^2 \mathbf{I}_K\right)$, where $\mathbf{I}_N$ denotes the identity matrix of size $N \times N$. Choosing conjugate Gaussian priors for $\mathbf{a}$ and $\mathbf{h}$ considerably simplifies the algorithm, since the resulting conditional distributions are also Gaussian. Here, σ_a^2 and σ_h^2 are fixed hyperparameters. The impulse response is normalized to avoid scale ambiguity (different values of amplitude and impulse response could provide the same convolution results) such that $\sigma_h^2 = 1$. Moreover, the proposed algorithm normalizes the ECG signals with different amplitude resolutions by their maximum R-peak amplitude such that $\sigma_a^2 = 1$ can cover all possible amplitude values. Conversely, the noise variance σ_n^2 is estimated together with the other unknown parameters using a hierarchical Bayesian model. For the prior of σ_n^2, we use an inverse gamma distribution $IG(\xi, \eta)$ as suggested in [30], where ξ and η are fixed hyperparameters providing a vague prior.

C. Posterior Distribution

The posterior distribution of the unknown parameters can be computed from the following hierarchical structure:

$$p(\boldsymbol{\theta}|\mathbf{x}) \propto p(\mathbf{x}|\boldsymbol{\theta})\, p(\mathbf{a}|\mathbf{b})\, p(\mathbf{b})\, p(\mathbf{h})\, p\left(\sigma_n^2\right). \tag{6}$$

The usual Bayesian estimators related to this posterior are the minimum mean square error (MMSE) estimator and the maximum a posteriori (MAP) estimator [32]. Due to the complexity of the posterior distribution given by (6), it is difficult to obtain closed-form expressions for these estimators. As a consequence, we propose to study an MCMC method, which generates samples asymptotically distributed according to the target distribution. The MMSE or MAP estimators of the unknown parameters are then computed using the generated samples. The main principles of MCMC methods can be found in [22]. The

Algorithm 1

set k = 1
while $k \leq K$ **do**
  sample b_k from $p\left(b_k|\mathbf{b}_{\sim J_d(k)}, \mathbf{a}_{\sim J_d(k)}, \mathbf{h}, \sigma_n^2, \mathbf{x}\right)$
  if $b_k = 1$ **then**
    sample a_k from $p\left(a_k|b_k = 1, \mathbf{b}_{\sim J_d(k)}, \mathbf{a}_{\sim J_d(k)}, \mathbf{h}, \sigma_n^2, \mathbf{x}\right)$
    set $\mathbf{b}_{J_d(k)\setminus k} = \mathbf{0}$
    set $k = k + d - 1$
  end if
  set $k = k + 1$
end while
sample $\mathbf{h}$ from $p\left(\mathbf{h}|\mathbf{b}, \mathbf{a}, \sigma_n^2, \mathbf{x}\right)$
sample σ_n^2 from $p\left(\sigma_n^2|\mathbf{b}, \mathbf{a}, \mathbf{h}, \mathbf{x}\right)$

PCGS generates samples distributed according to (6) and its procedure is given in detail in the next section.

IV. PCGS for Wave Extraction

A. Standard GS

To obtain samples from $p\left(\mathbf{b}, \mathbf{a}, \mathbf{h}, \sigma_n^2|\mathbf{x}\right)$, the standard Gibbs sampler (GS) iteratively generates samples from $p\left(\mathbf{b}|\mathbf{a}, \mathbf{h}, \sigma_n^2, \mathbf{x}\right)$, $p\left(\mathbf{a}|\mathbf{b}, \mathbf{h}, \sigma_n^2, \mathbf{x}\right)$, $p\left(\mathbf{h}|\mathbf{a}, \mathbf{b}, \sigma_n^2, \mathbf{x}\right)$, and $p\left(\sigma_n^2|\mathbf{a}, \mathbf{b}, \mathbf{h}, \mathbf{x}\right)$. However, as pointed out in [26], this GS is poorly suited to problems with local constraints because a constraint that excludes parts of the hypothesis space may inhibit convergence to $p\left(\mathbf{b}, \mathbf{a}, \mathbf{h}, \sigma_n^2|\mathbf{x}\right)$.

B. Partially Collapsed GS

In our case, the unknown parameter vector $\boldsymbol{\theta}$ is split into two parts, i.e., $(\mathbf{b}, \mathbf{a})$ that contains the constrained parameters and $\left(\mathbf{h}, \sigma_n^2\right)$ that contains the unconstrained parameters. To accelerate the convergence of the GS, we propose a PCGS that takes into consideration the local constraints affecting $\mathbf{b}$ and $\mathbf{a}$. More precisely, denote as $J_d(k)$, a right-hand neighborhood of k with length d, i.e., $J_d(k) = \{k, \ldots, k + d - 1\}$. Divide the wave indicator vector $\mathbf{b}$ and the wave amplitude vector $\mathbf{a}$ into two parts $\mathbf{b}_{J_d(k)} = [b_k, \ldots, b_{k+d-1}]^T$, $\mathbf{b}_{\sim J_d(k)} = [b_1, \ldots, b_{k-1}, b_{k+d}, \ldots, b_K]^T$, and $\mathbf{a}_{J_d(k)} = [a_k, \ldots, a_{k+d-1}]^T$, $\mathbf{a}_{\sim J_d(k)} = [a_1, \ldots, a_{k-1}, a_{k+d}, \ldots, a_K]^T$ [where the notation $\mathbf{b}_{\sim J_d(k)}$ denotes $\mathbf{b}$ without the components belonging to $J_d(k)$]. The proposed PCGS iteratively generates b_k and a_k according to the conditional distributions $p\left(b_k|\mathbf{b}_{\sim J_d(k)}, \mathbf{a}_{\sim J_d(k)}, \mathbf{h}, \sigma_n^2, \mathbf{x}\right)$ and $p\left(a_k|b_k, \mathbf{b}_{\sim J_d(k)}, \mathbf{a}_{\sim J_d(k)}, \mathbf{h}, \sigma_n^2, \mathbf{x}\right)$. The resulting algorithm is summarized in Algorithm 1, and is detailed in what follows, whereas the different conditional distributions are derived in the Appendix and in [33]. Note that the convergence of this sampler to the target distribution (6) directly results from [23] (see also [24] and [25] for applications of the PCGS). The reader is invited to consult [33] for interesting results showing a faster convergence of the PCGS when compared to the usual GS.

Indicators. The sampling distribution for b_k is a conditional distribution associated with the joint posterior $p\left(\mathbf{b}, \mathbf{a}, \mathbf{h}, \sigma_n^2|\mathbf{x}\right)$ marginalized with respect to the remaining parameters in the neighborhood $J_d(k) \setminus k = \{k + 1, \ldots, k + d - 1\}$. Thus, $\mathbf{b}_{J_d(k)}$ is not contained in the condition for b_k. The marginalization of the joint posterior cannot be analytically obtained with respect to $\mathbf{b}_{J_d(k)\setminus k} = [b_{k+1}, \ldots, b_{k+d-1}]^T$. Indeed, this conditional distribution can be calculated as $p\left(b_k|\mathbf{b}_{\sim J_d(k)}, \mathbf{a}_{\sim J_d(k)}, \mathbf{h}, \sigma_n^2, \mathbf{x}\right) = \sum_{\mathbf{b}_{J_d(k)\setminus k}} p(\mathbf{b}_{J_d(k)}|\mathbf{b}_{\sim J_d(k)}, \mathbf{a}_{\sim J_d(k)}, \mathbf{h}, \sigma_n^2, \mathbf{x})$. Thus, we propose to sample $\mathbf{b}_{J_d(k)}$ from $p\left(\mathbf{b}_{J_d(k)}|\mathbf{b}_{\sim J_d(k)}, \mathbf{a}_{\sim J_d(k)}, \mathbf{h}, \sigma_n^2, \mathbf{x}\right)$ and then use the b_k contained in the sample. Therefore, the sampling distribution for wave indicators is

$$p\left(\mathbf{b}_{J_d(k)}|\mathbf{b}_{\sim J_d(k)}, \mathbf{a}_{\sim J_d(k)}, \mathbf{h}, \sigma_n^2, \mathbf{x}\right) \propto \sigma_1 \exp\left(\frac{|\mu_1|^2}{2\sigma_1^2}\right) p(\mathbf{b})$$

with

$$\sigma_1^2 = \left(\frac{\left\|\mathbf{F}_{J_d(k)}\mathbf{b}_{J_d(k)}\right\|^2}{\sigma_n^2} + \frac{1}{\sigma_a^2}\right)^{-1}$$

$$\mu_1 = \frac{\sigma_1^2 \mathbf{b}_{J_d(k)}^T \mathbf{F}_{J_d(k)}^T \left(\mathbf{x} - \mathbf{F}_{\sim J_d(k)}\mathbf{B}_{\sim J_d(k)}\mathbf{a}_{\sim J_d(k)}\right)}{\sigma_n^2}$$

where $\mathbf{F}_{J_d(k)}$ denotes the columns of $\mathbf{F}$ indexed by $J_d(k)$, $\mathbf{F}_{\sim J_d(k)}$ denotes $\mathbf{F}$ without those columns, and $\mathbf{B}_{\sim J_d(k)}$ denotes the diagonal matrix diag $\left(\mathbf{b}_{\sim J_d(k)}\right)$ (see Appendix).

Amplitudes. Since $p(\mathbf{a})$ is a conjugate prior, we obtain

$$p\left(a_k|b_k = 1, \mathbf{b}_{\sim J_d(k)}, \mathbf{a}_{\sim J_d(k)}, \mathbf{h}, \sigma_n^2, \mathbf{x}\right) = \mathcal{N}\left(\mu_1, \sigma_1^2\right).$$

Note that the amplitude a_k is sampled only when $b_k = 1$, i.e., when a wave has been detected.

Waveform coefficients. Because $\mathbf{h}$ is a priori Gaussian, straightforward computations lead to

$$p\left(\mathbf{h}|\mathbf{b}, \mathbf{a}, \sigma_n^2, \mathbf{x}\right) = \mathcal{N}\left(\boldsymbol{\mu}_2, \boldsymbol{\Sigma}_2\right)$$

with

$$\boldsymbol{\mu}_2 = \frac{\boldsymbol{\sigma}_2^2 \mathbf{U}^T \mathbf{x}}{\sigma_n^2} \qquad \boldsymbol{\Sigma}_2 = \left(\frac{\mathbf{U}^T\mathbf{U}}{\sigma_n^2} + \frac{\mathbf{I}_{L+1}}{\sigma_h^2}\right)^{-1}$$

where $\mathbf{U}$ is the Toeplitz matrix of size $K \times (L + 1)$ with first row $[u_1 \ \mathbf{0}_L]$ and first column $\left[\mathbf{u}^T \ \mathbf{0}_L\right]^T$. Note that $\mathbf{Uh}$ is equivalent to $\mathbf{FBa}$. Thus, (3) can be represented as $\mathbf{x} = \mathbf{Uh} + \mathbf{n}$. As mentioned in Section III-A, scale ambiguity inherent to the convolution model is resolved by normalizing $\mathbf{h}$ every iteration.

Noise variance. The conditional distribution of the noise variance is the following inverse gamma distribution:

$$p\left(\sigma_n^2|\mathbf{b}, \mathbf{a}, \mathbf{h}, \mathbf{x}\right) = IG\left(\xi + \frac{K}{2}, \eta + \frac{1}{2}\|\mathbf{x} - \mathbf{FBa}\|^2\right).$$

C. P- and T-Wave Detection and Delineation Criteria

P- and T-wave detection and delineation are based on the estimated joint posterior distribution of wave indicators, wave amplitudes, and waveform coefficients. This posterior is computed from the histograms of the samples generated by the PCGS.

1) P- and T-Wave Detection: Unlike most of the approaches found in the literature, no rigid amplitude threshold is used to determine whether waves are representative or not. The posterior distribution of wave indicators carries information regarding the

probability of having a P- or T-wave at a given location. Thus, the detection results $\hat{\mathbf{b}}$ can be obtained with various degrees of certainty by using a local MAP strategy. Since there are at most one T-wave (P-wave) in each T-searching neighborhood (P-searching neighborhood), the proposed algorithm compares the highest estimated posterior probability from each neighborhood to a given probability threshold (γ_P for P-wave and γ_T for T-wave) in order to decide whether it is representative or not.[1] If the local MAP is higher than the threshold, the corresponding indicator location can be seen as the estimate wave location in this searching neighborhood. Note that the estimated indicator posterior probability at position k is defined as follows (the probability of having $b_k = 1$ equal to $\mathrm{E}[b_k]$, where $\mathrm{E}[\cdot]$ is the mathematical expectation since b_k is a binary random variable)

$$\hat{b}_{k,\mathrm{MMSE}} = \frac{1}{N_r}\sum_{t=1}^{N_r} b_k^{(N_{\mathrm{bi}}+t)} \tag{7}$$

where $b_k^{(t)}$ denotes the indicator at position k generated at iteration t, while N_r is the number of iterations and N_{bi} is the number of burn-in[2] iterations.

2) Estimation of Wave Amplitudes, Waveforms, and Noise Variance: For estimating, the wave amplitude a_k corresponding to a position k, where a P- or T-wave has been detected, we use the MMSE estimator of a_k conditionally upon $b_k = 1$

$$\hat{a}_{k,\mathrm{MMSE}} = \frac{1}{|\mathcal{T}_k|}\sum_{t\in\mathcal{T}_k} a_k^{(N_{\mathrm{bi}}+t)} \tag{8}$$

where $a_k^{(t)}$ denotes the kth entry of the amplitude vector $\mathbf{a}$ generated by the Markov chain at iteration t, $\mathcal{T}_k$ is the set of indices t of all iterations satisfying $b_k^{(t)} = 1$ excluding burn-in iterations. Note that $\hat{a}_{k,\mathrm{MMSE}}$ is calculated only when a P- or T-wave has been detected.

The MMSE estimators of the waveform coefficients $\mathbf{h}$ and the noise variance σ_n^2 are defined as

$$\hat{\mathbf{h}}_{\mathrm{MMSE}} = \frac{1}{N_r}\sum_{t=1}^{N_r} \mathbf{h}^{(N_{\mathrm{bi}}+t)} \tag{9}$$

$$\hat{\sigma_n^2}_{\mathrm{MMSE}} = \frac{1}{N_r}\sum_{t=1}^{N_r} \left(\sigma_n^2\right)^{(N_{\mathrm{bi}}+t)} \tag{10}$$

where $\mathbf{h}^{(t)}$ and $\left(\sigma_n^2\right)^{(t)}$ denote the samples of $\mathbf{h}$ and σ_n^2 generated at iteration t.

3) P- and T-Wave Delineation: Since the estimated waveform $\hat{\mathbf{h}}_{\mathrm{MMSE}}$ carries information about the wave morphology, we propose a delineation criterion that is based on the waveform estimate of each processing window. The waveform onset and end are estimated as either the first value of $\hat{\mathbf{h}}_{\mathrm{MMSE}}$ below the threshold (ζ_{Pon} and ζ_{Poff} for P waves, and ζ_{Ton} and ζ_{Toff} for T waves, see left part of Fig. 3) or the first local minimum of $\hat{\mathbf{h}}_{\mathrm{MMSE}}$ (see right part of Fig. 3). Since there is no universal rule to locate onsets and ends of waves, the delineation thresholds have been obtained by minimizing the error between estimates and published annotations. The following results have been obtained for the QTDB

$$\zeta_{\mathrm{Ton}} = 0.02\max(\hat{\mathbf{h}}_T) \qquad \zeta_{\mathrm{Toff}} = 0.1\max(\hat{\mathbf{h}}_T)$$
$$\zeta_{\mathrm{Pon}} = 0.05\max(\hat{\mathbf{h}}_P) \qquad \zeta_{\mathrm{Poff}} = 0.1\max(\hat{\mathbf{h}}_P).$$

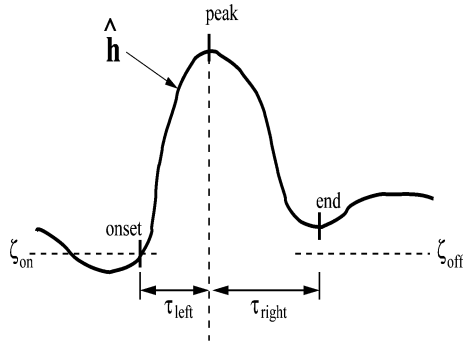

Fig. 3. Parameters of the wave delineation method.

The general flowchart for the proposed algorithm including preprocessing, PCGS, and wave delineation is shown in Fig. 4.

V. Simulation Results

Simulations were conducted to validate the proposed algorithm. First, we show some posterior distributions and estimation results for one typical example. Then, graphical evaluations and analytical results on an entire database are provided. Usually, the validation of the ECG wave detector or delineator is done using a manually annotated database. In this paper, we use one of the easily available standard databases, namely, the QTDB [27]. The QTDB includes 105 records from the widely used MIT–BIH arrhythmia database (MITBIH), the European ST-T database and some other well-known databases. This database was developed with the purpose of providing a wave-limit validation reference.

A. One Typical Example

The first simulations have been obtained by applying the proposed algorithm on the dataset "sele0136" of QTDB. This example has been chosen because signals from this data set present rhythm changes with obvious amplitude variations. The processing window length D has been set to ten beats, as in [20]. For each P- or T-wave search block, we have generated $N_{\mathrm{r}} = 100$ realizations according to the priors given in Section III with $\sigma_a^2 = 1$, $\sigma_h^2 = 1$, $\xi = 11$, and $\eta = 0.5$ (these are fixed hyperparameters that provide a noninformative prior). The value of λ in (5) has been fixed by dividing the number of R peaks within the processing window by the window length K. We considered $N_{\mathrm{bi}} = 40$ burn-in iterations and 60 iterations to compute the estimates.[3] Note that running 100 iterations of the proposed algorithm for a ten-beat ECG block sampled at $Fs = 250$ Hz

[1]The reader can consult [33] for details about threshold determination.

[2]The burn-in period corresponds to the first iterations of the sampler that are not used for estimating the unknown parameters.

[3]To determine the values of N_{bi} and N_{r}, we have implemented the multivariate potential scale reduction factor [34] (see [33] for details).

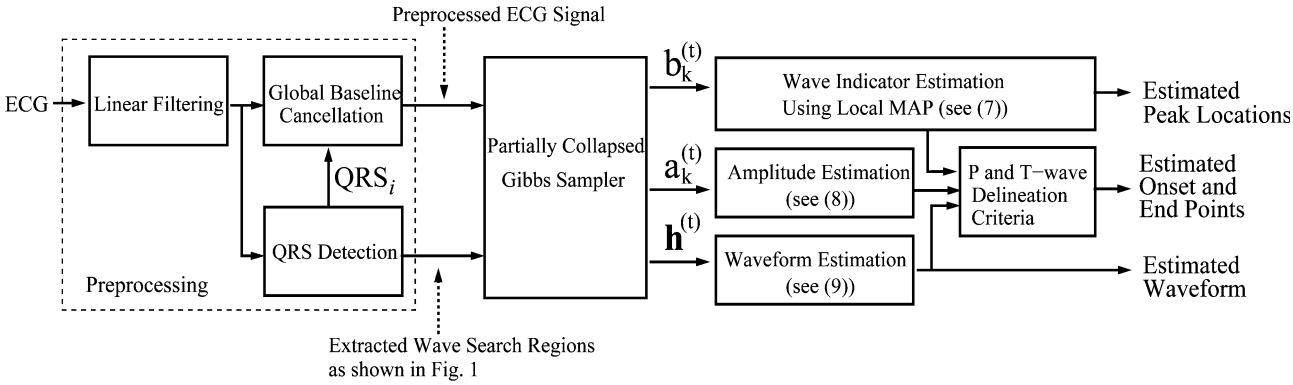

Fig. 4. General block diagram for the proposed P- and T-wave delineation algorithm.

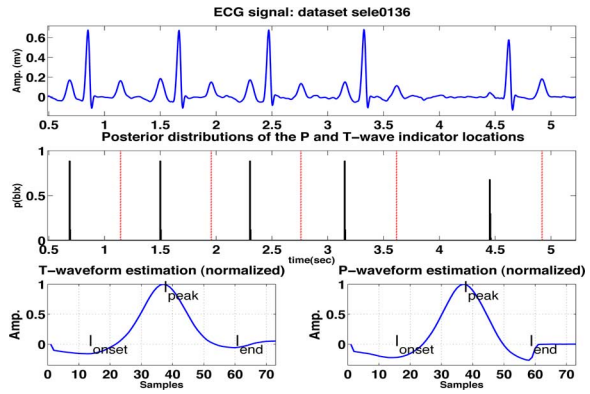

Fig. 5. Posterior distributions of the P- and T-wave indicator locations $p(\boldsymbol{b}_{\mathrm{P}})$ (middle black) and $p(\boldsymbol{b}_{\mathrm{T}})$ (middle dotted red) of an ECG signal portion from the QTDB "sele0136" (top), and the estimated P- and T-waveforms (bottom).

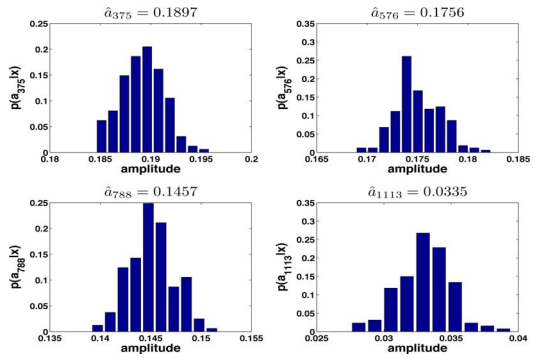

Fig. 6. Posterior distributions of the P-wave amplitudes $p(\mathbf{a}_k|\mathbf{x})$ at time instant 1.5, 2.3040, 3.1520, and 4.4520s.

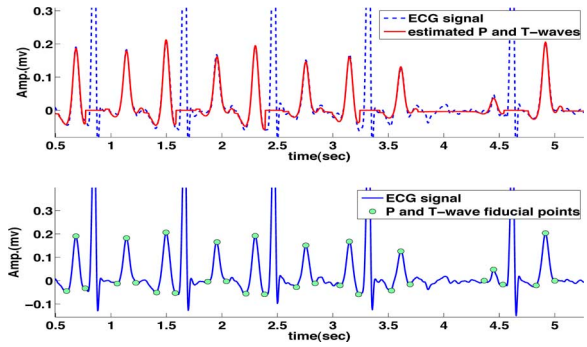

Fig. 7. On the top, real ECG signal from the QTDB "sele0136" (dashed blue) and estimated P- and T-waves (red); on the bottom, P- and T-wave delineation results.

(i.e., ECG signals lasting about 10 s) takes 13 s for a MATLAB implementation on a 3.0-GHz Pentium IV. However, these codes can be further optimized and converted to low-level languages.

As mentioned previously, the estimates of the unknown parameters are derived from their posterior distributions. Fig. 5 (middle) shows the posterior distributions of P- and T-wave indicator locations estimated using the last 60 Markov chain iterations. The posterior probability is very high for most of the actual P- and T-wave locations except for P-wave indicators around time instant 4.45. Indeed, the algorithm seems hesitant to locate P-wave indicators around this location. If we employ a simple rigid threshold on the entire block, it is likely that this wave indicator will be missed in the estimation. However, with the local maximum posterior strategy explained in Section IV, a relatively low value of γ_P can be used to ensure the detection of low magnitude waves without increasing false positives. Fig. 7 shows that the P-wave at time instant 4.45 is properly estimated.

Once we have obtained the P- and T-wave locations, the corresponding wave amplitudes can be estimated by using (8). Fig. 6 shows the posterior distributions $p(\mathbf{a}|\mathbf{x})$ and the estimates $\hat{\mathbf{a}}$ of P-wave amplitudes at time 1.5, 2.3040, 3.1520, and 4.4520 s. The estimated P- and T-waveforms determined using (9) are presented in Fig. 5 (bottom). As explained previously, P- and T-wave delineation is based on these estimated waveform coefficients. The estimated P- and T-waves and the delineation results of "sele0136" are illustrated in Fig. 7 (top) and Fig. 7 (bottom).

B. P- and T-Wave Delineation for Different Wave Morphologies

The proposed method estimates the P- and T-waveform shapes pointwise for each processing window. Therefore, it can adapt to various wave morphologies. This section shows some representative results obtained with the proposed method on different ECGs. The first example in Fig. 8(a) considers the QTDB

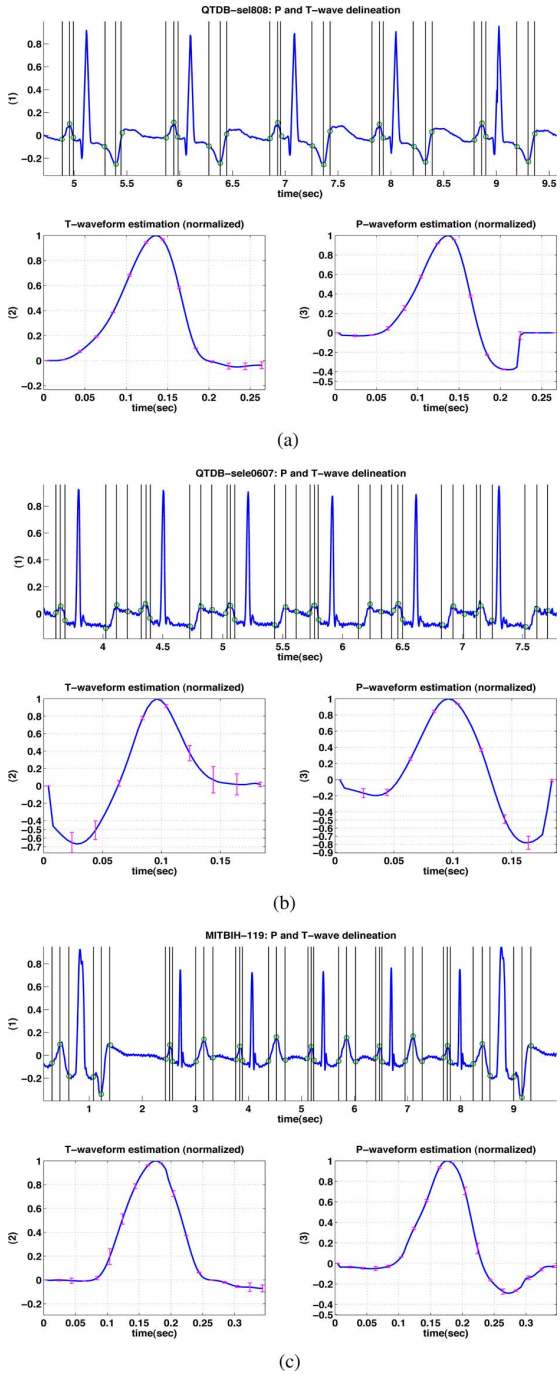

Fig. 8. Results of processing ECG datasets (a) "QTDB-sel808", (b) "QTDB-sele0607," and (c) "MITBIH-119". (1) Delineation results: the vertical lines show the manual annotations by an expert and the markers show the results of the proposed algorithm. (2) Mean (in blue) and standard deviations (in pink) of the estimated T-waveform for 1 min of signal length. (3) Mean (in blue) and standard deviations (in pink) of the estimated P-waveform for 1 min of signal length.

dataset "sel808", where T-waves are inverted. The second example considers noisy feeble P-waves and ascending T-waves from the QTDB dataset "sele0607". The results presented in Fig. 8(b) show that the proposed method provides good waveform estimation for noisy feeble waves. Fig. 8(c) shows an example of signals that contain premature ventricular contractions (PVCs) from the MITBIH dataset "119". As can be seen, the proposed method can handle nonmonotonic morphological abnormalities. Note in particular that the estimated T-wave of the sixth beat has been superimposed with the estimated P-wave of the seventh beat, which is in agreement with the presence of a unique wave in the non-QRS region between 8 and 9 s. Furthermore, with the help of the proposed signal model, the sudden T-wave amplitude inversions (the first and the last beats) have been detected, which is a nice property for the PVC detection problem. Finally, the reader is invited to consult [33], which shows delineation results obtained for other representative wave morphologies from the QTDB such as normal P- and T-waves ("sel16539"), feeble P-waves and prominent T-waves ("sel308"), and biphasic T-waves ("sel301") .

C. P and T-Wave Delineation: Analytical Results

The analytical evaluation of the P- and T-wave detection can be performed by calculating the sensitivity $Se = TP/(TP + FN)$ and positive predictivity $P^+ = TP/(TP + FP)$, where TP denotes the number of true positive detections (wave was present and was detected), FN stands for the number of false negative detections (wave was present but was missed), and FP stands for the number of false positive (wave was not present but was detected). The performance of wave delineation is measured by the average of errors m, which stands for the time differences between cardiologist annotations and results of the proposed method. The average of the intrarecording standard deviations denoted as s was also computed.

The validation results obtained with the PCGS-based delineator and the three other methods of [2], [7], and [18] on the QTDB are given in Table I.[4] It should be noted that the proposed algorithm requires an *a priori* QRS-detection step. All ECG signals used in this paper have been preprocessed by the QRS detection algorithm by Pan *et al.*, with an overall QRS detection result of $Se = 99.7\%$ and $P^+ = 99.6\%$. The beats, where QRS complexes were not well detected were excluded from the P- and T-wave evaluation.

The detection results on the QTDB show that the proposed method can detect with high sensitivity the P- and T-waves annotated by cardiologists in the ECG signals. We obtained a sensitivity of $Se = 98.93\%$ for the P-waves and a sensitivity of $Se = 99.81\%$ for the T-waves. These results are slightly better than the ones obtained with the other methods. As for the positive predictivity, we have obtained very good results since $P^+ = 97.40\%$ for the P-waves, and $T^+ = 98.97\%$ for the T-waves, which clearly outperforms the other algorithms evaluated in Table I. This is partly because the minimum-distance constraint in Bayesian detection reduces the probability of false positive. The delineation performance is also presented in Table I. The proposed algorithm can delineate the annotated P- and T-waves with mean errors m that do not exceed two samples (8 ms). The standard deviations s are around four samples for the P-wave and five samples for the T-wave, which is quite satisfactory.

[4]A comparison with the Kalman filter-based approach of [14] has also been conducted on representative ECG signals (see [33] for more details).

TABLE I
DELINEATION AND DETECTION PERFORMANCE COMPARISON IN THE QTDB. (N/A: NOT AVAILABLE)

Method	Parameters	P_{on}	P_{peak}	P_{end}	T_{on}	T_{peak}	T_{end}
PCGS (this work)	annotations	3176	3176	3176	1345	3403	3403
	$Se\,(\%)$	98.93	98.93	98.93	99.01	99.81	99.81
	$P^{+}\,(\%)$	97.40	97.40	97.40	96.07	98.97	98.97
	$m \pm s\,(ms)$	3.7±17.3	4.1±8.6	-3.1±15.1	7.1±18.5	1.3±10.5	4.3±20.8
WT [7]	annotations	3194	3194	3194	N/A	3542	3542
	$Se\,(\%)$	98.87	98.87	98.75	N/A	99.77	99.77
	$P^{+}\,(\%)$	91.03	91.03	91.03	N/A	97.79	97.79
	$m \pm s\,(ms)$	2.0±14.8	3.6±13.2	1.9±12.8	N/A	0.2±13.9	-1.6±18.1
LPD [2]	$Se\,(\%)$	97.70	97.70	97.70	N/A	99.00	99.00
	$P^{+}\,(\%)$	91.17	91.17	91.17	N/A	97.74	97.74
	$m \pm s\,(ms)$	14.0±13.3	4.8±10.6	-0.1±12.3	N/A	-7.2±14.3	13.5±27.0
Analysis of TU complexes [18]	$Se\,(\%)$	N/A	N/A	N/A	N/A	92.60	92.60
	$P^{+}\,(\%)$	N/A	N/A	N/A	N/A	N/A	N/A
	$m \pm s\,(ms)$	N/A	N/A	N/A	N/A	-12.0±23.4	0.8±30.3

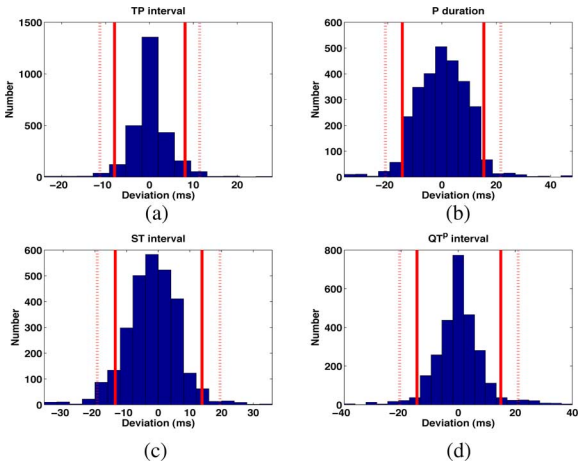

Fig. 9. Histograms of deviations between the results of the proposed automatic algorithm compared to the "gold standard" of manually measured annotations including (a) TP interval, (b) P-wave duration, (c) ST interval, and (d) QT^p interval. The vertical lines indicate the 95% (continuous red) and 99% (dashed red) confidence intervals.

Histograms of deviations between the results of the proposed algorithm compared to the "gold standard" of the manually measured annotations for TP interval ($\text{TP}_{\text{int}} = \text{T}_{\text{peak}} - \text{P}_{\text{peak}}$), P wave duration ($\text{P}_{\text{dur}} = \text{P}_{\text{onset}} - \text{P}_{\text{end}}$), ST interval ($\text{ST}_{\text{int}} = \text{S}_{\text{peak}} - \text{T}_{\text{end}}$), and QT^p interval ($\text{QT}^p_{\text{int}} = \text{Q}_{\text{peak}} - \text{T}_{\text{peak}}$) are presented in Fig. 9. These histograms are in agreement with the results of [35], which indicate that typical standard deviations for QT interval measurement are 20–30 ms. The deviations of the PCGS-based method are also similar to those obtained with the more recent technique studied in [14]. Smaller deviations (mostly below 8 ms) have been obtained for detections, which rely on peak points, i.e., TP_{int} and QT^p_{int}. For those detections, which rely on peak boundaries, the deviations are also in the acceptable range (mostly below 20 ms). Note that the proposed method focuses on P- and T-wave analysis. Thus, deviations of QRS locations are not considered here. Note also that due to its sequential nature, the proposed algorithm might have problems to handle signals containing several P- or T waves in the same research region, which can be observed for atrial fibrillation.

VI. CONCLUSION

This paper studied a Bayesian sampling algorithm performing joint P- and T-wave delineation and waveform estimation. Instead of deploying rigid detection and delineation criteria for all ECG time series, we used a local detection strategy and a flexible delineation criteria based on the estimation of P- and T waveforms in consecutive beat-processing windows. The main contributions of the paper as follows.

1) The introduction of a hierarchical Bayesian model for P- and T-wave delineation. This model is based on a modified Bernoulli–Gaussian sequence with minimum distance constraint for the wave locations and amplitudes, and appropriate priors for the wave impulse responses and noise variance.
2) The derivation of a PCGS allowing for the generation of samples distributed according to the posterior distribution associated to the previous hierarchical Bayesian model. The proposed PCGS overcomes the slow convergence problem encountered with the classical GS. To our knowledge, it is the first time this kind of simulation method is applied to ECG segmentation problems.
3) The proposed method allows for the simultaneous estimation of the P- and T-wave fiducial points and the P- and T-waveforms, which is rarely done by other ECG delineation methods.
4) The PCGS method allows for the determination of confidence intervals, which provide reliability information about the estimates (e.g., see error bars in Fig. 8). This could be useful for medical diagnosis.

The resulting algorithm was validated using the entire annotated QTDB. A comparison with other benchmark methods showed that the proposed method provides a reliable detection and an accurate delineation for a wide variety of wave morphologies. The most significant improvement was found in the P- and T-wave detection rate and the positive predictivity. In addition, the proposed method can provide accurate waveform estimation. Note, however, that the trade-off with the good PCGS detection and estimation performance is a higher computational cost, when compared to other more classical methods.

It is important to mention that the proposed PCGS also allows for observation of the waveform evolution among processing blocks. If we extract the T-wave search region on every other beat rather than successively, the proposed method can be directly used to perform TWA analysis. Indeed, the wave amplitude can be used to decide the presence or absence of TWA, while the waveform estimation can reflect the characterization of TWA waveform. This study is currently under investigation.

APPENDIX

SAMPLING DISTRIBUTIONS

Indicators. The sampling distribution for $\mathbf{b}_{J_d(k)}$

$$\begin{aligned} &p\left(\mathbf{b}_{J_d(k)}|\mathbf{b}_{\sim J_d(k)},\mathbf{a}_{\sim J_d(k)},\mathbf{h},\sigma_n^2,\mathbf{x}\right)\\ &\quad\propto p\left(\mathbf{b}_{J_d(k)},\mathbf{b}_{\sim J_d(k)},\mathbf{a}_{\sim J_d(k)},\mathbf{h},\sigma_n^2,\mathbf{x}\right)\\ &\quad\propto p\left(\mathbf{x}|\mathbf{b},\mathbf{a}_{\sim J_d(k)},\mathbf{h},\sigma_n^2\right)p\left(\mathbf{a}|\mathbf{b}\right)p\left(\mathbf{b}\right)\\ &\quad\propto\left[\int p\left(\mathbf{x}|\mathbf{b},\mathbf{a},\mathbf{h},\sigma_n^2\right)p\left(\mathbf{a}_{J_d(k)}|\mathbf{b}_{J_d(k)}\right)\mathrm{d}\mathbf{a}_{J_d(k)}\right]p\left(\mathbf{b}\right)\end{aligned}$$

Using the minimum-distance constraint, there must only be one nonzero wave indicator within the neighborhood $J_{d(k)}$, which is denoted as $k'\in J_{d(k)}$. Thus, $\mathbf{b}_{J_d(k)}$ can be split into two parts

$$\begin{cases} b_{k'}=1\\ b_m=0, \qquad m\in J_d\left(k\right)\setminus k'\end{cases}$$

where $J_d\left(k\right)\setminus k'$ denotes the set of locations within the neighborhood $J_d\left(k\right)$ excluding k'. The conditional distribution can be further developed by inserting all the prior distributions. By denoting as $\tilde{\mathbf{x}}=\mathbf{x}-\mathbf{F}_{\sim J_d(k)}\mathbf{B}_{\sim J_d(k)}\mathbf{a}_{\sim J_d(k)}$, we obtain:

$$\begin{aligned} &p\left(\mathbf{b}_{J_d(k)}|\mathbf{b}_{\sim J_d(k)},\mathbf{a}_{\sim J_d(k)},\mathbf{h},\sigma_n^2,\mathbf{x}\right)\\ &\quad\propto\left[\int\exp\left[-\frac{1}{2\sigma_n^2}\left\|\tilde{\mathbf{x}}-f_{k'}a_{k'}\right\|^2-\frac{a_{k'}^2}{2\sigma_a^2}\right]\mathrm{d}a_{k'}\right]p\left(\mathbf{b}\right)\\ &\quad\propto\left[\int\exp\left[-\frac{\left(a_{k'}-\mu_1\right)^2}{2\sigma_1^2}+\frac{\mu_1^2}{2\sigma_1^2}\right]\mathrm{d}a_{k'}\right]p\left(\mathbf{b}\right)\end{aligned}$$

where $f_{k'}=\mathbf{F}_{J_d(k)}\mathbf{b}_{J_d(k)}$ and μ_1,σ_1^2 are defined as follows:

$$\mu_1=\frac{\sigma_1^2f_{k'}^T\tilde{\mathbf{x}}}{\sigma_n^2},\sigma_1^2=\left(\frac{\left\|f_{k'}\right\|^2}{\sigma_n^2}+\frac{1}{\sigma_a^2}\right)^{-1}.$$

Finally, the indicator sampling distribution is

$$p\left(\mathbf{b}_{J_d(k)}|\mathbf{b}_{\sim J_d(k)},\mathbf{a}_{\sim J_d(k)},\mathbf{h},\sigma_n^2,\mathbf{x}\right)\propto\sigma_1\exp\left[\frac{\mu_1^2}{2\sigma_1^2}\right]p\left(\mathbf{b}\right).$$

Amplitudes. The sampling distribution for a_k is

$$\begin{aligned} &p\left(a_k|b_k=1,\mathbf{b}_{\sim J_d(k)},\mathbf{a}_{\sim J_d(k)},\mathbf{h},\sigma_n^2,\mathbf{x}\right)\\ &\quad\propto\int p\left(\mathbf{a}_{J_d(k)}|b_k=1,\mathbf{b}_{\setminus k},\mathbf{a}_{\sim J_d(k)},\mathbf{h},\sigma_n^2,\mathbf{x}\right)\mathrm{d}\mathbf{a}_{J_d(k)\setminus k}\\ &\quad\propto\int p\left(\mathbf{x}|b_k=1,\mathbf{b}_{\setminus k},\mathbf{a},\mathbf{h},\sigma_n^2\right)p\left(\mathbf{a}_{J_d(k)}|\mathbf{b}_{J_d(k)}\right)\mathrm{d}\mathbf{a}_{J_d(k)\setminus k}\end{aligned}$$

where $p\left(\mathbf{x}|\mathbf{b},\mathbf{a},\mathbf{h},\sigma_n^2\right)$ has been defined in (4) and $p\left(\mathbf{a}_{J_d(k)}|\mathbf{b}_{J_d(k)}\right)=\mathcal{N}\left(\mathbf{0},\sigma_a^2\mathbf{I}_{J_d(k)}\right)$. Consequently, straightforward computations (similar to those used for the indicator conditional distribution) yield

$$p\left(a_k|b_k=1,\mathbf{b}_{\sim J_d(k)},\mathbf{a}_{\sim J_d(k)},\mathbf{h},\sigma_n^2,\mathbf{x}\right)=\mathcal{N}\left(\mu_1,\sigma_1^2\right).$$

Waveform coefficients. The sampling distribution for $\mathbf{h}$ is

$$\begin{aligned} p\left(\mathbf{h}|\mathbf{b},\mathbf{a},\sigma_n^2,\mathbf{x}\right)&\propto p\left(\mathbf{x}|\mathbf{b},\mathbf{a},\mathbf{h},\sigma_n^2\right)p\left(\mathbf{h}\right)\\ &\propto\exp\left[-\frac{1}{2\sigma_n^2}\left\|\mathbf{x}-\mathbf{U}\mathbf{h}\right\|^2\right]\exp\left[-\frac{1}{2\sigma_h^2}\left\|\mathbf{h}\right\|^2\right]\end{aligned}$$

hence,

$$p\left(\mathbf{h}|\mathbf{b},\mathbf{a},\sigma_n^2,\mathbf{x}\right)=\mathcal{N}\left(\boldsymbol{\mu}_2,\boldsymbol{\Sigma}_2\right)$$

with

$$\boldsymbol{\mu}_2=\frac{\boldsymbol{\sigma}_2^2\mathbf{U}^T\mathbf{x}}{\sigma_n^2},\ \boldsymbol{\Sigma}_2=\left(\frac{\mathbf{U}^T\mathbf{U}}{\sigma_n^2}+\frac{\mathbf{I}_{L+1}}{\sigma_h^2}\right)^{-1}.$$

ACKNOWLEDGMENT

The authors would like to thank G. Kail and O. Sayadi for interesting exchanges and fruitful discussions regarding this paper, as well as M. Bugallo of Stony Brook University for helping them to fix the english grammar.

REFERENCES

[1] N. V. Thakor and Y. S. Zhu, "Application of adaptive filtering to ECG analysis: Noise cancellation and arrhythmia detection," *IEEE Trans. Biomed. Eng.*, vol. 38, no. 8, pp. 785–793, Aug. 1991.

[2] P. Laguna, R. Jané, and P. Caminal, "Automatic detection of wave boundaries in multilead ECG signals: Validation with the CSE database," *Comput. Biomed. Res.*, vol. 27, no. 1, pp. 45–60, Feb. 1994.

[3] P. Strumillo, "Nested median filtering for detecting T-wave offset in ECGs," *Electron. Lett.*, vol. 38, no. 14, pp. 682–683, Jul. 2002.

[4] I. S. N. Murthy and U. C. Niranjan, "Component wave delineation of ECG by filtering in the Fourier domain," *Med. Bio. Eng. Comput.*, vol. 30, pp. 169–176, Mar. 1992.

[5] I. S. N. Murthy and G. S. S. D. Prasad, "Analysis of ECG from pole-zero models," *IEEE Trans. Biomed. Eng.*, vol. 39, no. 7, pp. 741–751, Jul. 1992.

[6] C. Li, C. Zheng, and C. Tai, "Detection of ECG characteristic points using wavelet transforms," *IEEE Trans. Biomed. Eng.*, vol. 42, no. 1, pp. 21–28, Jan. 1995.

[7] J. P. Martínez, R. Almeida, S. Olmos, A. P. Rocha, and P. Laguna, "A Wavelet-based ECG delineator: Evaluation on standard databases," *IEEE Trans. Biomed. Eng.*, vol. 51, no. 4, pp. 570–581, Apr. 2004.

[8] S. S. Mehta, S. C. Saxena, and H. K. Verma, "Recognition of P and T waves in electrocardiograms using fuzzy theory," in *Proc. 1st Reg. Conf., IEEE Eng. Med. Bio. Soc.*, New Delhi, India, Feb. 1995, pp. 2/54–2/55.

[9] E. D. A. Botter, C. L. Nascimento, and T. Yoneyama, "A neural network with asymmetric basis functions for feature extraction of ECG P waves," *IEEE Trans. Neural Netw.*, vol. 12, no. 5, pp. 1252–1255, Sep. 2001.

[10] P. Trahanias and E. Skordalakis, "Syntactic pattern recognition of the ECG," *IEEE Trans. Pattern Anal. Mach. Intell.*, vol. 12, no. 7, pp. 648–657, Jul. 1990.

[11] J. Thomas, C. Rose, and F. Charpillet, "A multi-HMM approach to ECG segmentation," in *Proc. 18th IEEE Int. Conf. Tools Artif. Intell.*, Arlington, VA, Nov. 2006, pp. 609–616.

[12] G. D. Clifford and M. Villarroel, "Model-based determination of QT intervals," in *Proc. Comput. Cardiol.*, Valencia, Spain, Sep. 2006, vol. 33, pp. 357–360.

[13] O. Sayadi and M. B. Shamsollahi, "Model-based ECG fiducial points extraction using a modified extended Kalman filter structure," in *Proc. 1st Int. Symp. Appl. Sci. Biomed. Commun. Tech. (ISABEL)*, Aalborg, Denmark, Oct. 2008, pp. 1–5.

[14] O. Sayadi and M.B. Shamsollahi, "A model-based Bayesian framework for ECG beat segmentation," *J. Physiol. Meas.*, vol. 30, pp. 335–352, Mar. 2009.

[15] F. Gritzali and F. Gehed, "Detection of the P and T waves in an ECG," *Comput. Biomed. Res.*, vol. 22, pp. 83–91, Feb. 1989.
[16] V. S. Chouhan and S. S. Mehta, "Threshold-based detection of P and T-wave in ECG using new feature signal," *Int. J. Comput. Sci. Netw. Secur.*, vol. 8, no. 2, pp. 144–152, Feb. 2008.
[17] Z. Yang, L. Li, and J. Ling, "Approach to recognition of ECG P waves based on approximating functions," *J. Biomed. Eng.*, vol. 15, no. 2, pp. 120–122, Jun. 1998.
[18] J. A. Vila, Y. Gang, J. Presedo, M. Delgado, S. Barro, and M. Malik, "A new approach for TU complex characterization," *IEEE Trans. Biomed. Eng.*, vol. 47, no. 6, pp. 746–772, Jun. 2000.
[19] J. Dumont, A. I. Hernandez, and G. Carrault, "Improving ECG beats delineation with an evolutionary optimization process," *IEEE Trans. Biomed. Eng.*, vol. 57, no. 3, pp. 607–615, Mar. 2010.
[20] J. P. Martínez and S. Olmos, "Methodological principles of T Wave Alternans analysis: A unified framework," *IEEE Trans. Biomed. Eng.*, vol. 52, no. 4, pp. 599–613, Apr. 2005.
[21] Z. Elghazzawi and F. Gehed, "A knowledge-based system for arrhythmia detection," in *Proc. Comput. Cardiol.*, Indianapolis, IN, Sep. 1996, pp. 541–544.
[22] C. P. Robert and G. Casella, *Monte Carlo Statistical Methods*. New York: Springer-Verlag, 2004.
[23] D. A. Van Dyk and T. Park, "Partially collapsed Gibbs samplers: Theory and methods," *J. Acoust. Soc. Amer.*, vol. 103, pp. 790–796, 2008.
[24] D. Ge, "Décomposition impulsionnelle multi-source. Application aux signaux électromyographiques," Ph.D. dissertation, École Centrale de Nantes, France, Dec. 2009.
[25] G. Kail, C. Novak, B. Hofer, and F. Hlawatsch, "A blind Monte Carlo detection-estimation method for optical coherence tomography," in *Proc. IEEE Int. Conf. Acoust., Speech, Signal Process. (ICASSP)*, Taipei, Taiwan, Apr. 2009, pp. 493–496.
[26] G. Kail, J.-Y. Tourneret, F. Hlawatsch, and N. Dobigeon, "A partially collapsed Gibbs sampler for parameters with local constraints," in *Proc. IEEE Int. Conf. Acoust., Speech, Signal Process. (ICASSP)*, Dallas, TX, Mar. 2010, pp. 3886–3889.
[27] P. Laguna, R. Mark, A. Goldberger, and G. Moody, "A database for evaluation of algorithms for measurement of QT and other waveform intervals in the ECG," *Comput. Cardiol.*, vol. 24, pp. 673–676, Sep. 1997.
[28] J. Pan and W. J. Tompkins, "A real-time QRS detection algorithm," *IEEE Trans. Biomed. Eng.*, vol. 32, no. 3, pp. 230–236, Mar. 1985.
[29] V. S. Chouhan and S. S. Mehta, "Total removal of baseline drift from ECG signal," in *Proc. Int. Conf. Comput.: Theory Appl.*, Kolkata, India, Mar. 2007, pp. 512–515.
[30] N. Dobigeon, J.-Y. Tourneret, and M. Davy, "Joint segmentation of piecewise constant autoregressive processes by using a hierarchical model and a Bayesian sampling approach," *IEEE Trans. Signal Process.*, vol. 55, no. 4, pp. 1251–1263, Apr. 2007.
[31] D. Ge, E. L. Carpentier, and D. Farina, "Unsupervised Bayesian decomposition of multi-unit EMG recordings using tabu search," *IEEE Trans. Biomed. Eng.*, vol. 56, no. 12, pp. 1–9, Dec. 2009.
[32] H. L. Van Trees, *Detection, Estimation and Modulation Theory*. New York: Wiley, 1968.
[33] C. Lin, C. Mailhes, and J.-Y. Tourneret, "P and T-wave delineation in ECG signals using a Bayesian approach and a partially collapsed Gibbs sampler," IRIT/ENSEEIHT/TéSA, Tech. Rep., May 2010. [Online]. Available: http://lin.perso.enseeiht.fr/documents/TechReport032010.pdf.
[34] S. P. Brooks and A. Gelman, "General methods for monitoring convergence of iterative simulations," *J. Comput. Graphical Stat.*, vol. 7, no. 4, pp. 434–455, Dec. 1998.
[35] G. Moody, H. Koch, and U. Steinhoff, "The physionet/computers in cardiology challenge 2006: QT interval measurement," in *Proc. Comput. Cardiol.*, Valencia, Spain, Sep. 2006, pp. 313–316.

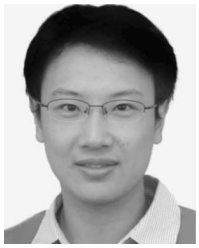

Chao Lin (S'10) received the the B.Sc. degree in telecommunication engineering from Beihang University, Beijing, China, in 2006, and the Eng. and M.Sc. degrees in signal processing from École Nationale Supérieure d'Électronique, d'Électrotechnique, d'Informatique et d'Hydraulique et des Télécommunication (ENSEEIHT), University of Toulouse, Toulouse, France, both in 2009.

He is currently working toward the Ph.D. degree at the University of Toulouse, where he is engaged Bayesian algorithms and Markov chain Monte Carlo methods for the analysis of electrocardiogram signals.

Corinne Mailhes (M'87) received the Eng. degree in electronics engineering and the Ph.D. degree in signal processing from École Nationale Supérieure d'Électronique, d'Électrotechnique, d'Informatique et d'Hydraulique et des Télécommunication (ENSEEIHT), University of Toulouse, France, in 1986 and 1990, respectively.

She is currently a Professor at ENSEEIHT and a member of the IRIT Laboratory (UMR 5505 of the CNRS) and of the TéSA Laboratory (http://www.tesa.prd.fr). Her research interests include statistical signal processing, with particular interests in spectral analysis, data compression, and biomedical signal processing.

Jean-Yves Tourneret (M'94–SM'08) received the Eng. degree in electrical engineering and the Ph.D. degree in signal processing from École Nationale Supérieure d'Électronique, d'Électrotechnique, d'Informatique et d'Hydraulique et des Télécommunication (ENSEEIHT), University of Toulouse, France, in 1989 and 1992, respectively.

He is currently a Professor at ENSEEIHT and a member of the IRIT Laboratory (UMR 5505 of the CNRS). His research interests include statistical signal processing with a particular interest to classification and Markov Chain Monte Carlo methods.

Dr. Tourneret was the Program Chair of the European Conference on Signal Processing, which was held in Toulouse in 2002. He was also a member of the Organizing Committee for the International Conference ICASSP 2006, which was held in Toulouse in 2006. He has been a member of different technical committees including the Signal Processing Theory and Methods committee of the IEEE SIGNAL PROCESSING SOCIETY (2001–2007). He is currently serving as an Associate Editor for the IEEE TRANSACTIONS ON SIGNAL PROCESSING.